Title	Synthesis of High-Quality Al-Doped ZnO Nanoink
Author(s)	Thu, Tran V.; Maenosono, Shinya
Citation	Journal of Applied Physics, 107(1): 14308-1-14308-6
Issue Date	2010-01-05
Type	Journal Article
Text version	publisher
URL	http://hdl.handle.net/10119/9189
Rights	Copyright 2010 American Institute of Physics. This article may be downloaded for personal use only. Any other use requires prior permission of the author and the American Institute of Physics. The following article appeared in Tran V. Thu and Shinya Maenosono, Journal of Applied Physics, 107(1), 14308- (2010) and may be found at http://link.aip.org/link/JAPIAU/v107/i1/p014308/s1
Description	

Synthesis of high-quality Al-doped ZnO nanoink

Tran V. Thu[1,2] and Shinya Maenosono[1,a)]
[1]School of Materials Science, Japan Advanced Institute of Science and Technology, 1-1 Asahidai, Nomi, Ishikawa 923-1292, Japan
[2]Faculty of Physics and Chemical Engineering, Le Quy Don Technical University, 100 Hoang Quoc Viet Street, Cau Giay District, Hanoi, Vietnam

(Received 25 September 2009; accepted 13 November 2009; published online 5 January 2010)

Al-doped ZnO (AZO) nanoparticles (NPs) have been synthesized via the thermal decomposition of metal acetylacetonate precursors in a nonoxygen and nonpolar solvent. Long-chain alkyl amines have been utilized to terminate the growth of AZO NPs and to stabilize them. The NPs have been characterized by a number of techniques as monocrystalline, exhibiting a hexagonal (wurtzite) structure with sizes from 8 to 13 nm. The composition of Al in the resulting NP is related solely to the composition of the reaction mixture and the size is controllable with the temperature of the reaction. The AZO NP dispersion has been proven to be stable over a 24 h period by dynamic light scattering measurements. The influence of the synthetic conditions, such as temperature, reaction time and the Al doping content, on the properties of NPs have also been investigated. An optically transparent AZO thin film was fabricated using the AZO nanoink by spin casting followed by annealing. The resulting film resistivity was measured to be 5.0×10^{-3} Ω cm. © *2010 American Institute of Physics*. [doi:10.1063/1.3273501]

I. INTRODUCTION

ZnO nanostructures are interesting materials as they have the potential to find applications in an enormous range of devices, such as solar cells,[1] catalysts,[2,3] varistors,[4,5] sensors,[6] optoelectronic devices,[7] light emitting diodes,[8] ultraviolet photodetectors,[9] transistors (including field-effect transistors),[10,11] printable transparent n-type semiconductors,[12] and even spintronic devices (diluted magnetic semiconductor).[13] ZnO exhibits a wide band gap of 3.37 eV at room temperature with a large exciton binding energy of 60 meV. ZnO has been doped with various elements to provide extrinsic optical, electric, and magnetic properties. Doping ZnO with B, Al, and Ga has been demonstrated to enhance the electron mobility of ZnO.[14] By introducing these high-valence elements into ZnO crystals, the oxide becomes nonstoichiometric, and it is possible to obtain both the visible transparency and high conductivity desired. This could be used to produce an attractive alternative to the traditional transparent conducting oxides, such as indium tin oxide, which is becoming both scarce and expensive.

ZnO nanoparticles (NPs) can be synthesized via many routes such as sol-gel,[15] ultrasonic-assisted sol-gel,[16] thermolysis,[17] sequential reduction-oxidation reaction,[18] microemulsion mediated synthesis,[19] mechanochemical processing,[20] coprecipitation,[21] sputtering,[22] hydrothermal synthesis,[23] and solvothermal synthesis.[24,25] Many efforts have been made to control the morphology, size, and growth of ZnO NPs.[26–30]

Although there have been many studies on the synthesis, characterization, and applications of Al-doped ZnO (AZO) films, there are only a few reports concerning the synthesis of AZO NPs. Highly crystallized AZO NPs can be synthesized by dry methods, such as vapor condensation,[31,32] spray pyrolysis,[33] or low-pressure spray pyrolysis.[34] Because high-temperature treatment is often necessary to obtain the final product, aggregation occurs and it is difficult to redisperse these NPs into a solvent for further fabrication. In addition, dry methods normally require intricate and synchronous reaction systems, which are costly to implement.

These obstacles could be overcome by synthesis in a solvent. Coprecipitation synthesis[35,36] is a rather simple and versatile route, in which the hydroxide of a metal is precipitated in a reaction between a metal precursor and a strongly alkaline solution. These are then converted to an oxide NPs by heat treatment. Organometallic or inorganic salts can be used as precursors. These NPs unfortunately exhibit unacceptably wide size distributions. Due to the amphoteric nature of compounds of Zn and Al, it is difficult to simultaneously obtain high yields and a precise Al doping content. The elemental composition of these NPs has not been reported in the literature so far. Hydrothermal[31,32] and sol-gel synthesizes[37] take advantage of short reaction times and low temperatures, and tend to yield a higher doping level than the evaporation/condensation methods. However, the resulting AZO NPs have a mean size larger than 30 nm and are severely aggregated. In addition, there is no information regarding their size distribution or dispersibility. AZO NPs could also be synthesized by the microwave-assisted polyol route,[38] which is relatively facile and low cost. However, the residual solvent (diethylene glycol) needs to be burned off with a series of post-treatment steps including a heat treatment. In summary, there have been no reports of a successful synthesis method to produce high quality AZO nanoinks.

For a NP to be used in the nanoinkjet printing of electronic devices, they must have a small size, narrow size distribution, good dispersibility and sufficient colloidal stability.

a)Author to whom correspondence should be addressed. Electronic mail: shinya@jaist.ac.jp.

Pyrolytic synthesis may prove to be a suitable method to produce AZO NPs with these characteristics. It has been successfully applied to the synthesis of many types of NPs such as FePt.[39] In this paper, ZnO and AZO NPs have been synthesized by the thermal decomposition of the appropriate acetylacetonate precursors. A new synthetic route has been proposed and applied to obtain high quality AZO NPs in high yield. The resulting AZO NPs have a small mean size, narrow size distribution, and good dispersibility, which make them suitable for use as a nanoink. A detailed study of the influence of reaction parameters and Al doping content on the structural characteristics of the NPs is also presented.

II. EXPERIMENTAL

A. Synthesis of ZnO and AZO NPs

The reagents were purchased from Sigma-Aldrich Corp., and the solvents, including cyclohexane, ethanol, chloroform, n-butylamine, and toluene, were obtained from Kanto Chemical Co., Inc. All were used without further purification. In a typical procedure for preparing AZO NPs, 20 mmol of oleylamine (OLA, technical grade, 70% with primary amine content >98%) and 20 mmol of 1-octadecene (ODE, technical grade, 90%) were loaded into a three-necked flask at room temperature. A solution was prepared by dispersing 1 mmol of zinc acetylacetonate hydrate [$Zn(acac)_2$, 99.995%] and the appropriate amount of aluminum acetylacetonate [$Al(acac)_3$, 99%] in toluene. The flask was purged at 100 °C for about 15 min in a temperature-controlled electromantle under an argon atmosphere. This was then heated to 330 °C for the standard experiment. Then, the $Zn(acac)_2/Al(acac)_3$ solution was rapidly injected into the OLA/ODE solution with vigorous magnetic stirring. The mixture was kept at this temperature for 60 min then cooled to room temperature. 30 ml ethanol was poured into the reaction mixture to precipitate the AZO NPs from the solution. After several hours at rest, the NPs were collected by centrifugation, followed by washing three times with ethanol. All analyses and characterizations were carried out on the NPs in this state.

B. Characterization

X-ray diffraction (XRD) patterns were obtained using a Rigaku RINT-2500 diffractometer (Cu $K\alpha$ radiation line $\lambda = 1.5408$ Å; 40 kV/100 mA) and were recorded at angles between 20° and 80°, with a scan rate of 0.01°/min. The XRD patterns were also analyzed using MDI JADE7 software, then the average crystallite sizes (D_{XRD}) were estimated from the (101) peak according to the Scherrer formula,

$$D_{XRD} = \frac{K\lambda}{B \cos \theta},$$

where $K = 0.9$ is the Scherrer constant; λ is the wavelength of the incident x-ray beam (1.5408 Å for Cu $K\alpha$ radiation); θ is the Bragg angle, and B is the full width at the half maximum (FWHM) in radians.

Transmission electron microscopy (TEM) samples were prepared by casting 10 μl of solution (ZnO or AZO NPs/$CHCl_3$/n-butylamine) onto a carbon-coated copper grid at room temperature and allowing the sample to evaporate slowly in air. Low-magnification TEM images were obtained using a Hitachi H-7100. High resolution TEM/energy dispersive x-ray (TEM-EDX) analyses and high-angle annular dark-field (HAADF) measurements were conducted using the JEOL JEM-ARM200F. Dynamic light scattering (DLS) measurements were conducted on a Malvern HPP5001 high performance particle sizer.

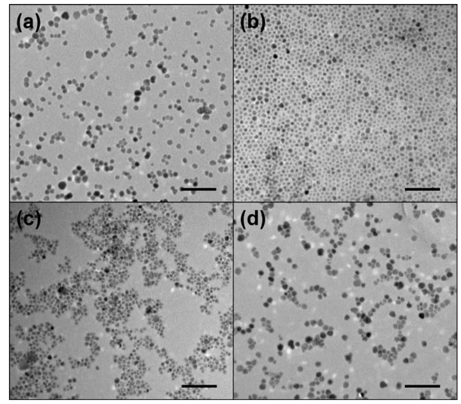

FIG. 1. TEM images of AZO NPs synthesized under different input molar ratios of $Al(acac)_3$ (a) 0 mol %, (b) 2.5 mol %, (c) 5.0 mol %, and (d) 10 mol %. Bar 100 nm.

III. RESULTS AND DISCUSSION

The TEM images of ZnO and AZO NPs synthesized under different input molar ratios, showed the ZnO and AZO NPs were basically spherical, as shown in Fig. 1. Among them, a majority of the ZnO and AZO NPs produced were hexagonal, and the average diameter of the NPs was in the 8–13 nm range. These NPs were uniform and well dispersed in nonpolar solvents, such as chloroform, toluene, or cyclohexane. No aggregation was observed, indicating the capping ligands were successfully attached to the surface of the NPs. The Al content in the AZO NPs seems to have no significant effect upon the average diameter and the size distribution of the NPs.

The small mean size of the AZO NPs obtained in these experiments can be explained using the LaMer model.[40] The formation of NPs in liquid phase is determined by two critical steps, the nucleation and the growth of the particles. By fostering the first step and inhibiting the second, monodispersed nanosized particles can be obtained. In this reaction, the sudden injection of stock solution into the three-necked flask causes the rapid decomposition of the acetylacetonate precursors due to the high temperature. This results in an increase in the nucleation rate and the sudden supersaturation of the solution with ZnO molecules. This means that most of the precursors are consumed during the nucleation to form numerous small crystallites. Then, they are rapidly capped by oleylamine to form stable colloidal NPs, resulting in their small size.

It is important to emphasize that the kinetics of the nucleation also strongly depends on the mass and heat transfer, especially when the temperature gradient is high and the

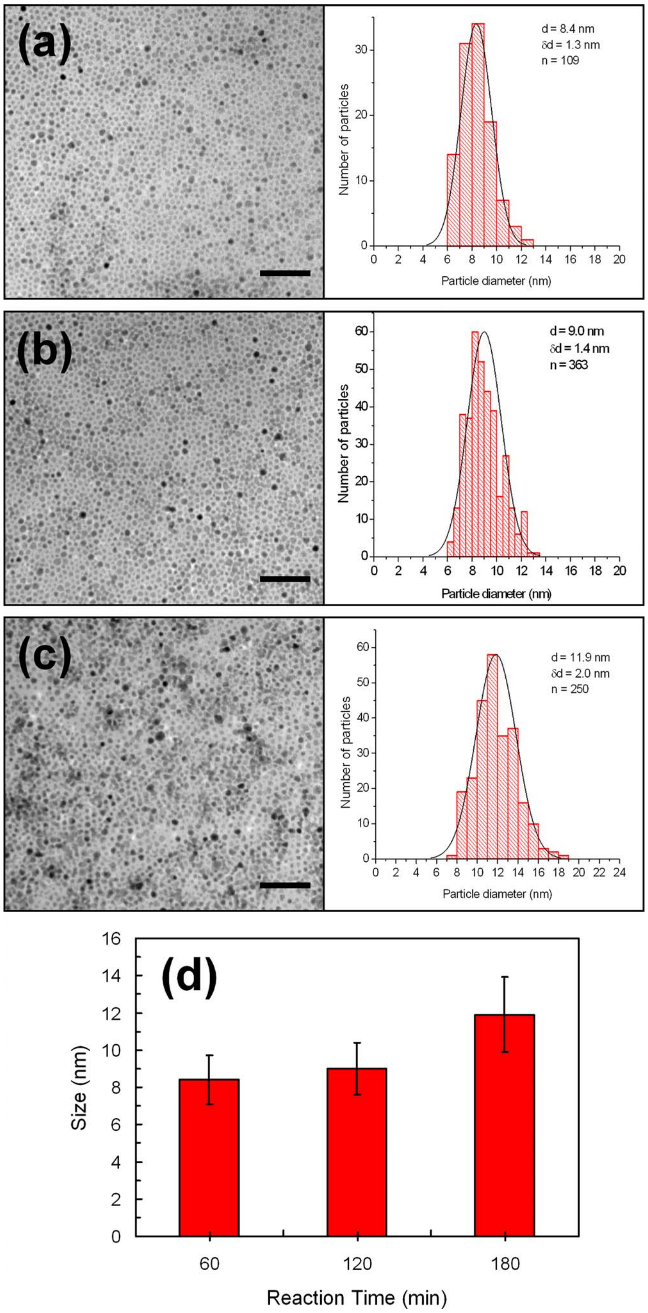

FIG. 2. (Color online) TEM images (right column) and size distributions (left column) of AZO NPs (2.5 input mol %) synthesized under different reaction times: (a) 60 min, (b) 120 min, and (c) 180 min. Bar 100 nm. (d) Mean size and standard deviation plotted vs the reaction time.

reaction volume is large. During the reaction, a minority of NPs continue to be formed after the initial nucleation, whereas the existing NPs will continue to grow. Some of NPs which have high surface energy (for example, those NPs that are not sufficiently capped by surface ligands) will also aggregate to form larger particles. Therefore, when the reaction time is increased from 60 to 180 min, both the mean particle size and the standard deviation increase as shown in Fig. 2. Fortunately, these increases are quite small [Fig. 2(d)]. This suggests that the nucleation step is the determining factor over the size and shape. Increasing the reaction time beyond 180 min causes the solvent to evaporate to the point it tends to polymerize uncontrollably.

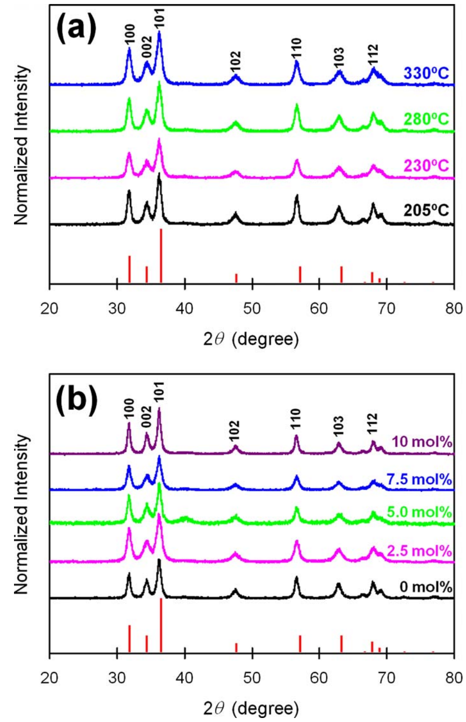

FIG. 3. (Color online) (Color online) (a) XRD patterns of AZO NPs (5 input mol %) synthesized under different temperatures 205, 230, 280, and 330 °C. (b) XRD patterns of AZO NPs synthesized under different input molar ratios of $Al(acac)_3$: 0, 2.5, 5.0, 7.5, and 10 mol %. Red bars represent the reference XRD pattern of ZnO (PDF #01–070–2552).

XRD patterns of ZnO and AZO NPs synthesized at different temperatures [Fig. 3(a)] and with different molar ratios of Al [Fig. 3(b)] indicate only the hexagonal structure, the wurtzite phase, is present. In the XRD patterns of AZO NPs, the presence of other phases, such as aluminum oxide (Al_2O_3), gahnite ($ZnAl_2O_4$), and pure Al, was not detected. These results suggest that Al atoms are successfully substituted into Zn atom positions and there is no significant variation in the crystalline structure of the resulting NPs. Because Al^{3+} might be promptly reduced to Al^0 in the presence of oleylamine, which could be a reductant at high temperature, the generation of aluminum oxide was suppressed. XRD patterns of AZO NPs (5 mol % input molar ratio) synthesized at a variety of temperatures (205, 230, 280, and 330 °C) are shown in Fig. 3(a). The presence of ZnO wurtzite phase over

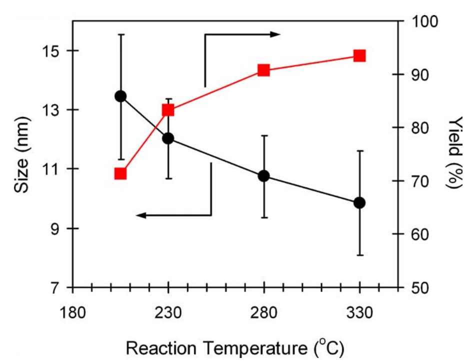

FIG. 4. (Color online) (Color online) Reaction temperature dependences of mean size (black circles) and reaction yield (red squares) of AZO NPs (5 input mol %).

TABLE I. The (101) peak position, d-spacing of the (101) plane, FWHM of the (101) peak and the mean crystalline size estimated by Scherrer formula and from the TEM images of AZO NPs (5 input mol%) synthesized under different temperatures.

Temp (°C)	(101) peak (degree)	d_{101}-spacing (Å)	FWHM (degree)	D_{XRD} (nm)	D_{XRD} (nm)
203	36.21	2.4788	0.600	13.3	13.4
230	36.22	2.4781	0.639	12.4	12.0
280	36.22	2.4781	0.655	12.1	10.7
330	36.26	2.4755	0.670	11.9	9.9

TABLE II. TEM-EDX analysis results of the AZO NPs synthesized under different input molar ratios of Al(acac)$_3$.

Input molar ratio of Al(acac)$_3$ (mol%)	Al content (atomic%)
0	0.0
2.5	0.0
5.0	0.7
7.5	1.7
10.0	4.1

the entire range of temperatures means the reaction can be carried out at under different temperatures to give consistent products of different sizes. When the reaction temperature was increased from 205 to 330 °C, the mean size decreases from 13.4 to 9.9 nm and the reaction yield increased from 71% to 93% (Fig. 4). The relationship between reaction yield and temperature comes from the endothermic nature of the decomposition reaction. These results suggest that to gain a high reaction yield, the reaction should take place at higher temperature. In addition, an increase in the intensity of the XRD main peak (101) was observed as the reaction temperature increased. This indicates that higher temperatures favor higher crystalline quality.

A summary of the crystal characteristics of the AZO NPs (5 mol %) synthesized at different temperature is given in Table I. The increase in the reaction temperature results in a slight shift in the (101) peak toward wider angle. This result suggests that the Al content slightly increases as the reaction temperature increases as the ionic radius of Al (53.5 pm) is much smaller than that of Zn (74 pm). Thus, the substitution of Zn by Al should decrease the d-spacing. However, the change in the Al content was not detected by EDX analyses possibly due to the difference being too small. On the other hand, the FWHM of the (101) peak also increases with an increase in the reaction temperature. This indicates that the mean crystallite size (D_{XRD}) is decreasing as the reaction temperature increases. At the same time, estimates of the mean size from the TEM image (D_{TEM}) also decrease as mentioned above. These results suggest that the nucleation rate increases as the temperature increases. As seen in Table I, the D_{XRD} and the D_{TEM} are similar, indicating the NPs are nearly monocrystalline. These results indicate NPs synthesized at higher temperatures will be superior for use as nanoinks. However, the reaction temperature was limited by the boiling point of the mixture, including the solvent and the capping ligand. Based on the boiling points of 1-octadecene (179 °C) and oleylamine (~350 °C) and the composition of their mixture (1:1), the reaction temperature should not be higher than 330 °C.

The TEM-EDX spectrum of AZO NPs (Al 10 mol %, reaction temperature 330 °C) is shown in Fig. 5. The copper peaks are due to the TEM grid. Note that the EDX spectrum was obtained from only a few dozen NPs. The presence of aluminum in the spectrum indicates that Al has been doped into the ZnO NPs. Table II summaries the TEM-EDX analyses results of the ZnO and AZO NPs synthesized with different molar ratios of Al:Zn. The minimum molar ratio, at which Al can be detected, was 5 mol % and resulted in an Al content of 0.7 at. %. When the molar ratio of Al in the reaction mixture is increased from 2.5 to 10 mol %, the actual Al content increases from 0 to 4.1 at. % as shown in Fig. 6. This suggests that the doping of Al into ZnO NPs was more efficient better at higher reaction molar ratios, and that AZO NPs with yet higher Al doping levels could be synthesized. HAADF images of AZO NPs (10 mol %) are shown in Fig. 7. The image on the left shows the AZO NPs are uniform. The boundary between NPs can be clearly seen, indicating good stability and no aggregation. The magnified image on the right shows a single hexagonal AZO NP with a size of about 12 nm. The atomic planes are arranged periodically without grain boundaries indicating it is a single crystal.

To evaluate the dispersibility of the NPs, the ZnO and AZO NPs were redispersed in nonpolar solvents, such as chloroform, cyclohexane, or toluene, with a minimum concentration of 10 mg ml^{-1}. These solutions were almost col-

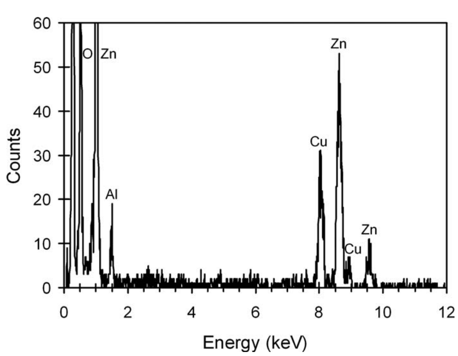

FIG. 5. TEM-EDX spectrum of AZO NPs (10 input mol%). Al content was detected as 4.1 at. %.

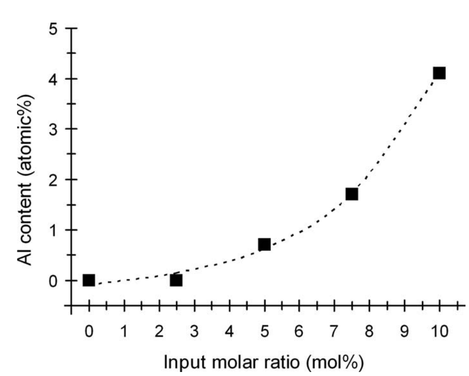

FIG. 6. Al content plotted vs the input molar ratio of Al(acac)$_3$. Dashed line corresponds to the single exponential fitting curve.

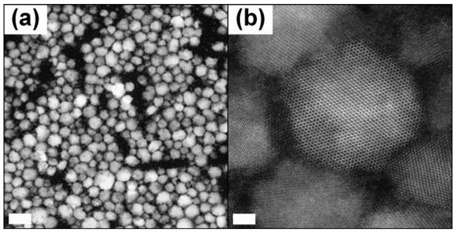

FIG. 7. HAADF images of AZO NPs (10 input mol %). (a) low-magnification (bar 20 nm) and (b) high-magnification (bar 2 nm).

orless and transparent as shown in Fig. 8. It means that there was no aggregation nor precipitation observed at ambient conditions. These results agree with the TEM images showed in the above sections (Figs. 1 and 2). The average hydrodynamic diameter (D_{DLS}) and the dynamic stability of the NP dispersion were examined for the AZO NPs (5 mol %) by DLS measurements. As shown in Fig. 9, the dispersion was stable after 1 h of storage, and its stability started to decrease only slightly after 24 h of storage. However, neither precipitation nor aggregation was observed by naked eye even after this time. A discrepancy between D_{TEM} and D_{DLS} could be explained based on the difference in nature between these two techniques: TEM measures "static" diameters (the size of the bare NPs deposited on the grids), while DLS measures "dynamic" diameters (the size of NPs with ligands under Brownian motion in solution). As expected, the static diameter is smaller than the dynamic one. Considering oleylamine is roughly 2 nm in length, the DLS results indicate that the AZO NPs were well dispersed in the solvent without aggregation at least for 1 day even at such a high concentration.

Finally, the AZO thin film was fabricated by spin casting the AZO nanoink [Al 10 mol %, solid concentration 5 wt %, solvent 9:1 (vol/vol) mixture of hexane and octane] onto a Si substrate at 800 rpm. Subsequently, the AZO thin film was annealed for 1 h in air at 450 °C. The film thicknesses of the as-cast and annealed samples were measured as 83 and 73 nm, respectively, by using a Dektak profilometer. The volume shrinkage of the annealed film indicates that the organic ligands were effectively removed. The surface morphology of the AZO thin film was analyzed by SEM. Figure 10 shows the SEM images of the AZO film before and after the annealing. The granular surface observed in the as-cast film was significantly smoothed after the annealing indicating the AZO NPs were sintered. The annealed film shows an average transmittance of about 90% in the visible region. The film

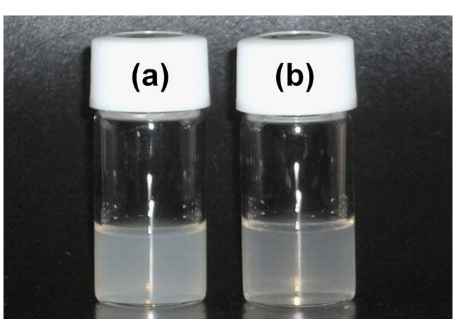

FIG. 8. (Color online) Photos of AZO NPs dispersed in chloroform at concentration of 10 mg/mL. (a) AZO NPs (10 input mol %) and (b) ZnO NPs.

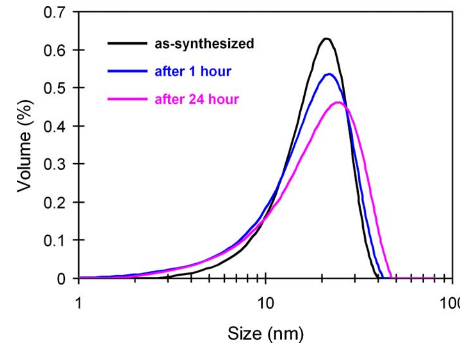

FIG. 9. (Color online) Temporal change of the size distribution of AZO NPs (5 input mol %) dispersed in chloroform measured by DLS.

resistivities were measured at ten different positions by using a four-point probe method. In consequence, the average resistivity was calculated to be 5.0×10^{-3} Ω cm (standard deviation 1.6×10^{-3} Ω cm), which is ten times as large as the resistivities (the order of 10^{-4} Ω cm) of sputtered AZO films (thicknesses were larger than 150 nm).[41,42] These results indicate that our AZO nanoink is promising for practical use.

IV. CONCLUSION

ZnO and AZO NPs were synthesized by the solvothermal decomposition of the respective acetylacetonate precursors with high reaction yield. All of the ZnO and AZO NPs exhibited the hexagonal, wurtzite structure and the presence of Al-contained compounds were not detected. Increasing the reaction temperature improved the crystallinity and afforded higher yields of the AZO NPs. The variation of Al content did not significantly influence the phase structure or the crystalline quality. The composition of the NPs corresponded to the molar ratio of precursors in the reaction mixture. Increasing of Al content up to 10 mol % had no significant effect upon the average diameter, size, or shape of NPs. The characteristics of NPs were dominated by the initial nucleation. The average diameter of the ZnO and AZO NPs were in the 8–13 nm range, which is much smaller than those in existing reports synthesized using the same method. This may be a result of the beneficial doping of Al into the ZnO crystal structure. ZnO and AZO NPs obtained were well dispersed in nonpolar solvents at various concentrations. An electrically conductive and optically transparent AZO thin film was fabricated using the AZO nanoink via a wet process.

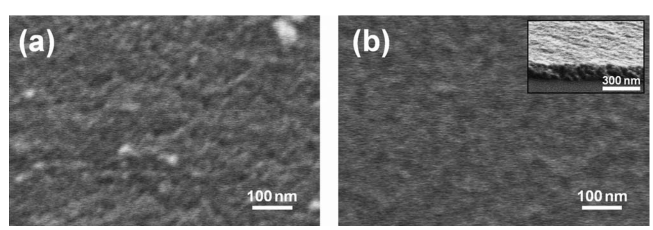

FIG. 10. SEM images of the AZO thin film (a) before and (b) after the annealing. The inset in (b) shows the cross-sectional SEM micrograph of the annealed film.

ACKNOWLEDGMENTS

The authors would like to thank the Vietnamese Government for a 322 scholarship. Mr. Noriaki Endo (JEOL) is thanked for his TEM-EDX analysis. We thank Dr. Derrick Mott for his carefully reading of, and useful comments about, the manuscript. This work is partly supported by a grant from the Hosokawa Powder Technology Foundation.

[1] Z. S. Wang, C. H. Huang, Y. Y. Huang, Y. J. Hou, P. H. Xie, B. W. Zhang, and H. M. Cheng, Chem. Mater. **13**, 678 (2001).
[2] G. M. Hamminga, G. Mul, and J. A. Moulijn, Chem. Eng. Sci. **59**, 5479 (2004).
[3] M. L. Curri, R. Comparelli, P. D. Cozzli, G. Mascolo, and A. Agostiano, Mater. Sci. Eng., C **23**, 285 (2003).
[4] M. Singhai, V. Chhabra, P. Kang, and D. O. Shah, Mater. Res. Bull. **32**, 239 (1997).
[5] R. N. Viswanath, S. Ramasamy, R. Ramamoorthy, P. Jayavel, and T. Nagarajan, Nanostruct. Mater. **6**, 993 (1995).
[6] J. Xu, Q. Pan, Y. Shun, and Z. Tian, Sens. Actuators B **66**, 277 (2000).
[7] X. L. Guo, H. Tabata, and T. Kawai, J. Cryst. Growth **237–239**, 544 (2002).
[8] D. C. Kim, W. S. Han, H. K. Cho, B. H. Kong, and H. S. Kim, Appl. Phys. Lett. **91**, 231901 (2007).
[9] Y. Jin, J. Wang, B. Sun, J. C. Blakesley, and N. C. Greenham, Nano Lett. **8**, 1649 (2008).
[10] B. J. Norris, J. Anderson, J. F. Wager, and D. A. Keszler, J. Phys. D: Appl. Phys. **36**, L105 (2003).
[11] B. Sun and H. Sirringhaus, Nano Lett. **5**, 2408 (2005).
[12] S. K. Volkman, B. A. Mattis, S. E. Molesa, J. B. Lee, A. F. Vornbrock, T. Bakhishev, and V. Subramanian, Tech. Dig. - Int. Electron Devices Meet. **2004**, 769.
[13] S. J. Pearton, D. P. Norton, M. P. Ivill, A. F. Hebard, J. M. Zavada, W. M. Chen, and I. A. Buyanova, IEEE Trans. Electron Devices **54**, 1040 (2007).
[14] C. Klingshirn, Phys. Status Solidi B **244**, 3027 (2007).
[15] L. Spanhel and M. A. Anderson, J. Am. Chem. Soc. **113**, 2826 (1991).
[16] D. Qian, J. Z. Jiang, and P. L. Hansen, Chem. Commun. (Cambridge) **2003**, 1078.
[17] S. H. Choi, E. G. Kim, J. Park, K. An, N. Lee, S. C. Kim, and T. Hyeon, J. Phys. Chem. B **109**, 14792 (2005).
[18] P. D. Cozzoli, A. Kornowski, and H. Weller, J. Phys. Chem. B **109**, 2638 (2005).
[19] S. Hingorani, V. Pillai, P. Kumar, M. S. Multani, and D. O. Shah, Mater. Res. Bull. **28**, 1303 (1993).
[20] T. Tsuzuki and P. G. McCormick, Scr. Mater. **44**, 1731 (2001).
[21] J. E. Rodríguez-Paéz, A. C. Caballero, M. Villegas, C. Moure, P. Durán, and J. F. Fernández, J. Eur. Ceram. Soc. **21**, 925 (2001).
[22] M. Selmi, F. Chaabouni, M. Abaab, and B. Rezig, Superlattices Microstruct. **44**, 268 (2008).
[23] R. C. Wang and C. C. Tsai, Appl. Phys. A: Mater. Sci. Process. **94**, 241 (2009).
[24] J. F. Liu, Y. Y. Bei, H. P. Wu, D. Shen, J. Z. Gong, X. G. Li, Y. W. Wang, N. P. Jiang, and J. Z. Jiang, Mater. Lett. **61**, 2837 (2007).
[25] M. Salavati-Niasari, F. Davar, and M. Mazaheri, Mater. Lett. **62**, 1890 (2008).
[26] J. Buha, I. Djerdj, and M. Niederberger, Cryst. Growth Des. **7**, 113 (2007).
[27] Z. Zhang, M. Lu, H. Xu, and W. S. Chin, Chemistry (Weinheim, Ger.) **13**, 632 (2007).
[28] T. Andelman, R. Gong, M. Polking, M. Yin, I. Kuskovsky, G. Neumark, and S. O'Brien, J. Phys. Chem. B **109**, 14314 (2005).
[29] F. Yang, J. K. Jin, Q. Chen, J. Z. Sun, and M. Wang, Mater. Lett. **62**, 3579 (2008).
[30] M. L. Kahn, M. Monge, V. Collière, F. Senocq, A. Maisonnat, and B. Chaudret, Adv. Funct. Mater. **15**, 458 (2005).
[31] T. Strachowski, E. Grzanka, W. Lojkowski, A. Presz, M. Godlewski, S. Yatsunenko, H. Matysiak, R. R. Piticescu, and C. J. Monty, J. Appl. Phys. **102**, 073513 (2007).
[32] R. R. Piticescu, R. M. Piticescu, and C. J. Monty, J. Eur. Ceram. Soc. **26**, 2979 (2006).
[33] K. C. Hsiao, S. C. Liao, and Y. J. Chen, Mater. Sci. Eng., A **447**, 71 (2007).
[34] D. Hidayat, T. Ogi, F. Iskandar, and K. Okuyama, Mater. Sci. Eng., B **151**, 231 (2008).
[35] S. Suwanboon, P. Amornpitoksuk, A. Haidoux, and J. C. Tedenac, J. Alloys Compd. **462**, 335 (2008).
[36] J. Nayak, S. Kimura, S. Nozaki, H. Ono, and K. Uchida, Superlattices Microstruct. **42**, 438 (2007).
[37] K. J. Chen, T. H. Fang, F. Y. Hung, L. W. Ji, S. J. Chang, S. J. Young, and Y. J. Hsiao, Appl. Surf. Sci. **254**, 5791 (2008).
[38] E. Hammarberg, A. Prodi-Schwab, and C. Feldmann, J. Colloid Interface Sci. **334**, 29 (2009).
[39] S. Saita and S. Maenosono, Chem. Mater. **17**, 3705 (2005).
[40] V. K. LaMer and R. H. Dinegar, J. Am. Chem. Soc. **72**, 4847 (1950).
[41] K. H. Kim, K. C. Park, and D. Y. Ma, J. Appl. Phys. **81**, 7764 (1997).
[42] H. Zhu, E. Bunte, J. Hüpkes, H. Siekmann, and S. M. Huang, Thin Solid Films **517**, 3161 (2009).